

# Curvelet-based method for orientation estimation of particles

Jouni Sampo<sup>a,b</sup>, Jouni Takalo<sup>a,c</sup>, Samuli Siltanen<sup>a</sup>, Matti Lassas<sup>a</sup>, Arttu Miettinen<sup>c</sup>, Jussi Timonen<sup>c</sup>

<sup>a</sup>*Department of Mathematics and Statistics, University of Helsinki, Finland*

<sup>b</sup>*Department of Mathematics and Physics, Lappeenranta University of Technology, Finland*

<sup>c</sup>*Department of Physics, University of Jyväskylä, Finland*

---

## Abstract

A method based on the curvelet transform is introduced for estimating from two-dimensional images the orientation distribution of small anisotropic particles. Orientation of fibers in paper is considered as a particular application of the method. Theoretical aspects of the suitability of this method are discussed and its efficiency is demonstrated with simulated and real images of fibrous systems. Comparison is made with two traditionally used methods of orientation analysis, and the new curvelet-based method is shown to perform clearly better than these traditional methods.

*Keywords:* curvelet, orientation, multiscale, anisotropic, fiber

---

## 1. Introduction

Orientation analysis of complex patterns is usually done by applying the Fourier transform [1] or gradient based methods like the structure tensors [2, 3, 4, 5]. Relative strengths of different orientations are measured, e.g., by investigating the magnitudes of Fourier-transform coefficients, usually in polar coordinates. However, during the last two decades, more sophisticated transforms, especially the wavelet transform [6], have become popular in many fields where Fourier transforms have traditionally been applied. Moreover, during the last decade, transforms like the curvelet, contourlet and shearlet transform have been developed and have proved to be well suited for some applications [7, 8, 9, 10]. The basis functions of these new transforms are tightly localized in both space and frequency domain, and have in

addition an angle (i.e., orientation) parameter that makes them promising tools for orientation analysis.

We use in this work the orientation of fibers in paper as the basic application and framework. This choice was made because data to be analyzed in this application are common and challenging. Therefore, if the methods developed work well in this case, they will probably work in many other (similar) applications such as, e.g., determination of the orientation of fibers or nanofibrils in reinforced composites [5, 11]. Furthermore, in papermaking industry it would be advantageous to have a good orientation-analysis method for on-line measurements during the manufacturing process (paper webs move up to 2000 m/min).

This article is organized as follows. In the second section we discuss the data typically related to the present application. In the third section the curvelet transform together with a few relevant theorems are introduced. Thereafter, in the fourth section, the curvelet method for orientation distribution is described. In the last section we apply this method to numerically generated networks of fibers and to a newsprint and organic-fiber sample, and compare the results to those achieved by other, previously used, methods of orientation analysis.

## 2. Optical imaging of fibers

In the paper making process wood fibers, mineral fillers, and other additives together form the basic structure of paper. The properties of paper depend essentially on how fibers are distributed. For example, orientation difference in separate layers of paper affects its bending stiffness, and such a difference between the two surfaces of paper makes it curved [12]. For this reason, it should be important in papermaking to be able to measure and to thereby facilitate control of fiber orientation in the paper web.

Fibers in paper form a more or less random network with predominantly planar orientation of fibers. As an off-line measurement, it is possible to study also the three-dimensional fiber structure of paper with tomographic imaging [13], but this is slow and the sample needs to be very small. With CCD cameras large areas of paper can be imaged fast, but these images mostly reveal the planar orientation of fibers only. Fortunately such information is often enough in practice. In an optimal case, determination of fiber orientation would enable on-line adjustment of the paper-making process. With currently available CCD cameras the whole paper web in suitable locations

of the paper machine can be imaged on-line, but then the resolution of the recorded images would not be high enough for analysis of fiber orientation. However, part of the web can be imaged with high resolution, and as camera technology keeps on developing rapidly, orientation analysis of the whole paper web is expected to become feasible fairly soon.

To make fibers more clearly visible in paper, through illumination is preferred over reflection images. Figure 1 exemplifies a typical image, found by through illumination, from which the orientation should be determined. Notice that fibers seem to be clearly visible. The light passing through paper is,

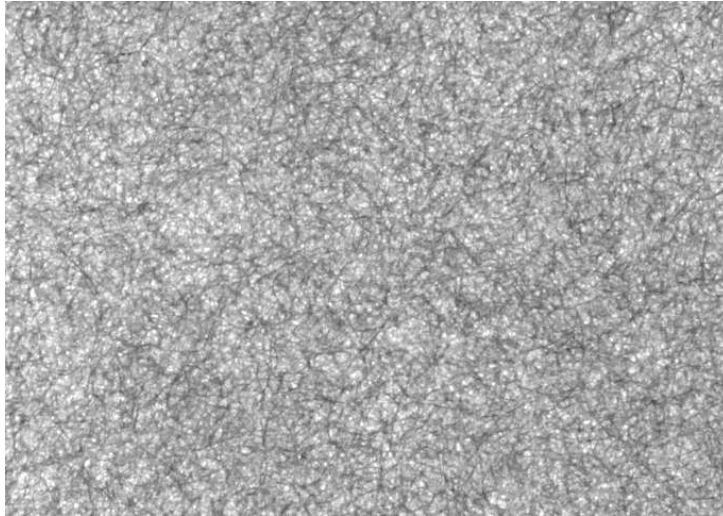


Figure 1: An optical image of paper with through illumination.

however, strongly scattered by the abundant fiber-air interfaces (wet paper is more transparent due to a better match of the dielectric properties of water and fibers), and therefore only the fibers that are close to the outlet surface can in practice be detected. We can demonstrate the 'diffusive' passage of light across paper by partly eclipsing the light source with a metal tape. In a thick paper the edge of the tape appears much more blurred than in a thin paper (see Fig. 2). It is evident that, with through illumination, only near-surface orientation can be determined from the images, which must be taken into account in practical applications.



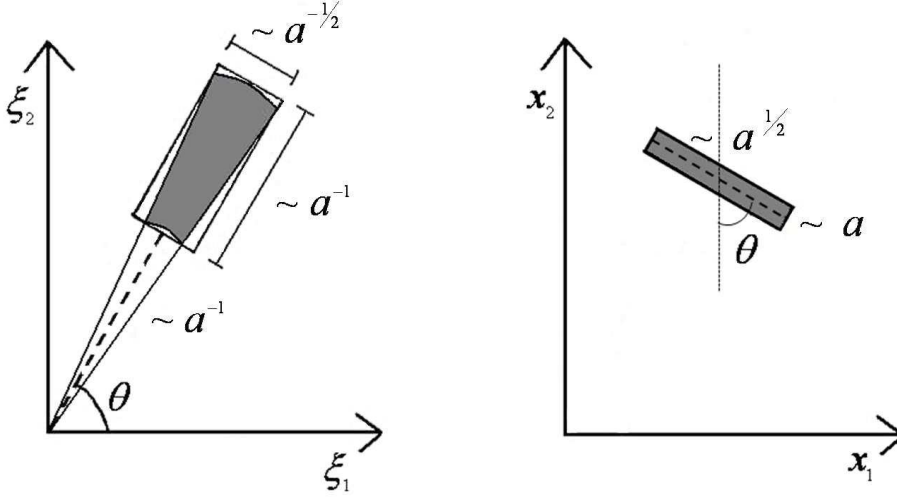


Figure 3: Left: Support of  $\hat{\gamma}_{ab\theta}$  in the frequency domain. Right: The area that contains most of the 'energy' of  $\gamma_{ab\theta}$ .

Now a rotation parameter,  $\theta \in [0, 2\pi)$ , and a translation parameter,  $b \in \mathbb{R}^2$ , are included so as to achieve a definition for the whole *curvelet*  $\gamma_{ab\theta}$ :

$$\gamma_{ab\theta}(x) = \gamma_{a00}(\mathbf{R}_{-\theta}(x - b)), \quad \text{for } x \in \mathbb{R}^2, \quad (3)$$

where  $R_\theta$  is the matrix of planar counter-clockwise rotation by the angle  $\theta$ . The curvelet transform  $\Gamma_f(a, b, \theta)$  of  $f$  is then defined by

$$\Gamma_f(a, b, \theta) := \langle \gamma_{ab\theta}, f \rangle = \int_{\mathbb{R}^2} f(x) \gamma_{ab\theta}(x) dx \quad (4)$$

for all  $0 < a < a_0$  and  $b \in \mathbb{R}^2$  and  $\theta \in [0, 2\pi)$ .

We remark that the curvelet transform has an inverse transform as well, although we do not need it in our application.

Because of the compact support of  $\hat{\gamma}_{ab\theta}$ , the support of  $\gamma_{ab\theta}$  cannot be compact. However, the following lemma provides information about the essential localization of  $\gamma_{ab\theta}$ . See [16] for the proof and Figure 3 for an illustration.

**Lemma 3.1.** *For each  $N = 1, 2, \dots$  there is a constant  $C_N$  such that*

$$\left| \frac{\partial^{\nu_1 + \nu_2} \gamma_{ab\theta}(x)}{\partial x_1^{\nu_1} \partial x_2^{\nu_2}} \right| \leq \frac{C_N a^{-3/4 - \nu_1 - \nu_2}}{1 + \|\mathbf{D}_{1/a} \mathbf{R}_{-\theta}(x - b)\|^{2N}}, \quad (5)$$

where  $D_{1/a} = \text{diag} \left( \frac{1}{a}, \frac{1}{\sqrt{a}} \right)$ .

It is evident from Figure 3 that the rotation parameter  $\theta$  is the angle between the  $x_2$  axis and the major orientation axis of  $\gamma_{ab\theta}$ . The *parabolic scaling law* of the aspect ratio of the area is suitable for our purposes. If we take a piece of smooth curve with a length of about  $a$ , then the whole piece will fit into a rectangle with the side lengths  $a$  and  $a^{1/2}$ . In our application such a piece of curve corresponds to an edge of the fiber, and therefore parabolic scaling gives, in some sense, the optimal size of the localizing window in every scale.

We can think of  $\gamma_{ab\theta}$  as a sensor that tries to detect if there is a fiber with orientation  $\theta$  in the neighborhood of  $b$ . If  $f$  now denotes a 2D image by a CCD camera, then the inner product  $\langle f, \gamma_{ab\theta} \rangle$  presents the response of sensor  $\gamma_{ab\theta}$ . A small value of parameter  $a$  means that we 'zoom' into a part of a fiber, while its bigger values can embed a whole fiber. If there is no fiber with orientation angle  $\theta$  located at point  $b$ , the value of  $|\langle f, \gamma_{ab\theta} \rangle|$  is very small.

Let us point out that the parabolic scaling law is the main difference between curvelets and wave packets (or the FBI transform). The latter display an isotropic type of scaling for essential localization, and therefore, in the present application, the transform can depend on more than one fiber, which eventually can make interpretation of the transform more difficult. However, a wave-packet transform can sometimes solve problems for which curvelets apply [14, 17], so the possibility is not excluded that it would work here also. In a wider sense, curvelets are sometimes even classified as wave packets.

### 3.2. Decay of the transform

Let us define *cartoon images* roughly as real-valued functions  $f(x_1, x_2)$  of two variables that are piecewise smooth with the smooth areas separated by smooth curves. The function  $f$  or its derivatives may have jump discontinuities along those curves.

The curvelet transform (and its variants) can approximate cartoon images with very few coefficients [8, 9, 10]. To explain this in more detail, let  $S$  denote a part of a curve separating domains of smoothness of  $f$ . The approximation property stems from the fact that  $|\langle f, \gamma_{ab\theta} \rangle|$  decays very fast when *either* the essential support of  $\gamma_{ab\theta}$  does not intersect  $S$ , *or* the orientation angle  $\theta$  differs from the tangent direction of  $S$  near the point  $b$ .

We can use the above decay property as a tool in the orientation analysis of fibers. In this section we will present two theorems related to the decay

rate of the curvelet transform, as a justification that this transform is a good candidate for analyzing fiber orientation. The theorems are not expressed in their most general forms since we focus here on a particular application.

**Theorem 3.2.** *Assume that  $b \in S$ . If the curve  $S$  is  $C^2$ -smooth with bounded second derivative inside  $B(b, r)$  for some  $r > 0$ , and if  $f$  is  $C^2(B(b, r) \setminus S)$  smooth with bounded second-order derivatives, then there exists a constant  $C < \infty$  such that, for all  $a, b$ , and  $\theta$ ,*

$$\left| \int_{\mathbb{R}^2} f(x) \gamma_{ab\theta}(x) dx \right| \leq \begin{cases} Ca^{3/4} & , \quad \hat{\theta} < Ca^{1/2} \\ C \frac{a^{3/4}}{\theta^3} & , \quad \hat{\theta} \geq Ca^{1/2} \end{cases} \quad (6)$$

*holds. Here  $\hat{\theta}$  is the angle between the tangent of  $S$  at  $b$  and the major orientation axis of  $\gamma_{ab\theta}$ .*

Theorem 3.2 states that  $|\langle f, \gamma_{ab\theta} \rangle|$  decays fast when the orientation of  $\gamma_{ab\theta}(x)$  departs from that of  $S$ . This decay estimate is well-known (presented in [9] for contourlets). For curvelets a proof can be found in [18], where the more general Theorem 14 includes this case.

However, Theorem 3.2 concerns only discontinuities of  $f$  on  $S$ . Because of the blurring effect explained in Section 2, it might be interesting also to know what happens to the transform if  $f$  is a bit smoother on  $S$ . (Another practical example is the X-ray image of a solid ball; it is continuous but not continuously differentiable.) Some research on this problem has been reported in [16].

**Theorem 3.3.** *Let us assume that  $b \in S$ ,  $\alpha > 0$ , and  $\beta > 0$ . If for some  $r > 0$  inside the ball  $B(b, r)$ , curve  $S$  is linear,  $f$  is uniformly  $C^\alpha(B(b, r))$  smooth and uniformly  $C^\beta(B(b, r))$  smooth in the direction of  $S$ , then there exists a  $C < \infty$  such that, for all  $a, b$ , and  $\theta$ ,*

$$\left| \int_{\mathbb{R}^2} f(x) \gamma_{ab\theta}(x) dx \right| \leq \begin{cases} Ca^{3/4+\alpha} & , \quad \hat{\theta} < Ca^{1/2} \\ Ca^{3/4} \left(\frac{a}{\theta}\right)^\beta & , \quad \hat{\theta} \geq Ca^{1/2} \end{cases} \quad (7)$$

*holds. Here  $\hat{\theta}$  is the angle between the tangent of  $S$  in  $b$  and the major axis of  $\gamma_{ab\theta}$ .*

The proof of Theorem 3.3 is postponed to Appendix A. It is evident that if  $\beta > 2\alpha$  the estimate for small angles is always bigger than that for large angles.

The above theorems only considered the case  $b \in S$ . They would be quite similar for  $b$  close to  $S$ . When the distance between  $b$  and  $S$  increases, Lemma 3.1 implies that  $|\Gamma_f(a, b, \theta)|$  decays rapidly. With the assumptions of Theorem 3.2, this is shown as Theorem 15 in [18].

In this article we consider only the curvelet transform, although the contourlet or shearlet transforms would probably work as well since they share most of the properties of the curvelet transform.

### 3.3. Estimate for the distribution of particle orientations

The theorems in the previous section already indicated that  $|\Gamma_f(a, b, \theta)|$  has a large value if  $\gamma_{ab\theta}$  is oriented similarly to a fiber.

The fact that a proper sampling of parameters  $a$ ,  $b$ , and  $\theta$  leads to a tight frame for  $L^2(\mathbb{R}^2)$  gives us an idea how to use the values  $|\langle f, \gamma_{ab\theta} \rangle|$  as a measure for orientation strength. The tight-frame property means that, with a proper discretization of  $a$ ,  $b$ , and  $\theta$ ,

$$\|f\|_2^2 = \sum_b |\langle f, \phi_b \rangle|^2 + \sum_{a,b,\theta} |\langle f, \gamma_{ab\theta} \rangle|^2 \quad (8)$$

with some functions  $\phi_b$ . These functions are restricted to low frequencies and are therefore not interesting to us in the present application. Details of  $\phi_b$  and discretizations of  $a$ ,  $b$ , and  $\theta$  can be found in [8]. Moreover,

$$f = \sum_b \langle f, \phi_b \rangle \phi_b + \sum_{a,b,\theta} \langle f, \gamma_{ab\theta} \rangle \gamma_{ab\theta}. \quad (9)$$

The definition of  $\gamma_{ab\theta}$  in [8] is a bit more complicated than the one introduced above, but all the essential properties of  $\gamma_{ab\theta}$  are the same.

The idea of the orientation-strength estimator is the following. Equations (8) and (9) imply that  $|\langle f, \gamma_{ab\theta} \rangle|^2$  measures how important the features related to a fixed value of parameter  $\theta$  are in  $f$ . Theorem 3.3 relates these features to edges that are oriented similarly to  $\gamma_{ab\theta}$ .

Discretization of  $\theta$  limits how accurately we can measure the orientation of fibers. However, in orientation analysis we do not have to restrict ourselves to any discretization of  $\theta$ , but we can argue in the following way: We can compare the importance of orientation at  $\theta = 0$  for different rotated versions of  $f(x)$ . Nothing limits the number of rotations we can use. We note that this kind of approach can be used in principle, in practice we still rotate  $\gamma$

instead of  $f$  since that rotation has to be done only once, but  $f$  changes in each analysis.

If the size of the particles is known, it is natural to consider only some fixed scales. Especially if there exist some features in bigger or smaller scales than the particle size, whose orientation distribution we are interested in, inclusion of too big or too small scales  $a$  in the final estimator may give rise to artifacts in the results. In the translation parameter  $b$  there is no need for restrictions. Finally, our estimate for the orientation distribution is then given by

$$S(\theta) := \frac{\sum_{a \in I} \sum_{b \in J_a} |\langle f, \gamma_{ab\theta} \rangle|^2}{\int_0^\pi \sum_{a \in I} \sum_{b \in J_a} |\langle f, \gamma_{ab\theta} \rangle|^2 d\theta}, \quad (10)$$

where index set  $I$  for scales depends on the resolution and size of the particles in the image and index set  $J_a$  depends on the implementation. We would also like to remark that a similar formalism would apply in the framework of continuous curvelets [15]. This 'semi-discrete' approach was chosen here because it is the one we used in tests made with the help of the CurveLab Toolbox (made by Candès, Demanet and Ying) that implements a discrete curvelet transform. In our tests we always used two subsequent scales, i.e.,  $I = \{C, C\sqrt{2}\}$  with constant  $C$  that depends on the resolution. For each scale CurveLab uses a regular rectangular grid points as the translation index set  $J_a$ , i.e.,  $J_a = \{R_\theta(C_1 l a, C_2 k a^{1/2})^\top : (l, k) \in \mathbb{Z}^2\}$  with  $C_1$  and  $C_2$  constant.

#### 4. Comparison with other methods

So as to get reference to the new curvelet-based orientation analysis developed above we compared its results with those of previously used methods.

As the first traditional method we used a direct Fourier-analysis (FFT)-based method [1]. In this method one simply computes the average of absolute values of the 2D Fourier-transform coefficients of  $f$  along radial lines. Similarly to our curvelet-based method, low frequencies are neglected in the analysis. The second traditional method was the so-called structure-tensor (ST) method [2, 3, 4, 5] that is one of the gradient methods developed recently. ST tries to find a direction  $\theta_m$  in which the  $L^2$  norm of the directional derivative is maximized. This method has two essential parameters: the size of the moving window that restricts the region considered at a time, and the thresholding value that removes the regions of weak orientation from the analysis.

#### 4.1. Results

We applied the curvelet-based method and the two traditional methods to three different images. These images were chosen so that they were not very sharp and were complex enough so as to be able to distinguish the capacity of the methods to determine orientation distributions. The first image was a numerically generated network of fibers with prescribed distribution of fiber orientations (mean 30 degrees and standard deviation 45 degrees). This network was generated using a deposition model in which fibers, sampled from specific length, diameter and orientation distributions, were let to fall towards a flat substrate until collision with solid objects (fibers and/or substrate) caused their movement to cease [19]. An image of the network is shown in Fig. 4, and the results for fiber orientation in this figure as given by the three methods are shown in Fig. 7 together with the prescribed (known) orientation distribution. All distributions are normalized to unit area (angles in radians).

The second image was of newsprint paper. It was taken such that the vertical direction made an angle of about 60 degrees towards the paper-machine direction (MD), which, for newsprint paper, is the dominant direction of fiber orientation. No other prior knowledge about the orientation distribution was available. The image, taken through an optical microscope with a CCD camera, is shown in Fig. 5, and the orientation distributions determined from this image with the three methods are shown in Fig.8.

The third image was that of organic nanofibrils taken with an atomic force microscope (AFM) (see Fig. 6). The orientation distributions of this image, determined by the three methods, are shown in Fig. 9.

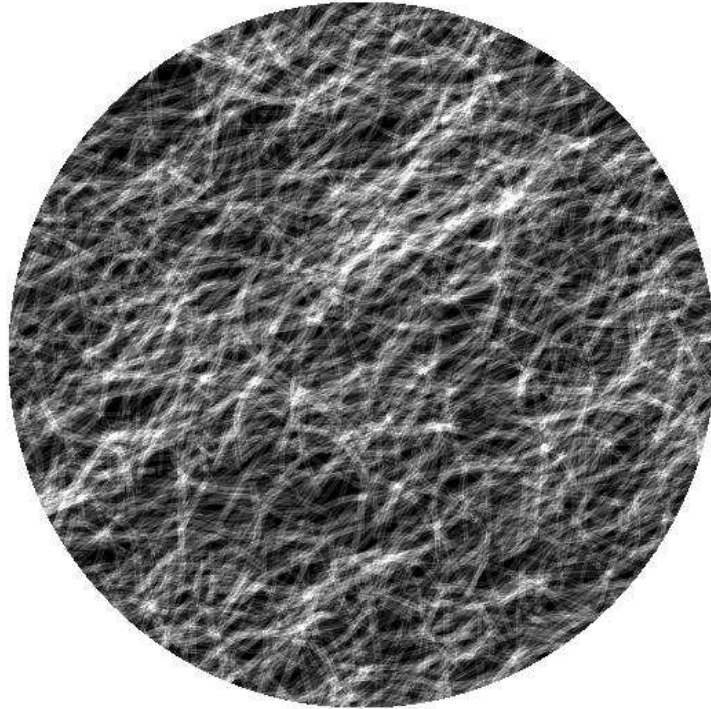


Figure 4: An image of a numerically generated (by deposition) network of fibers.

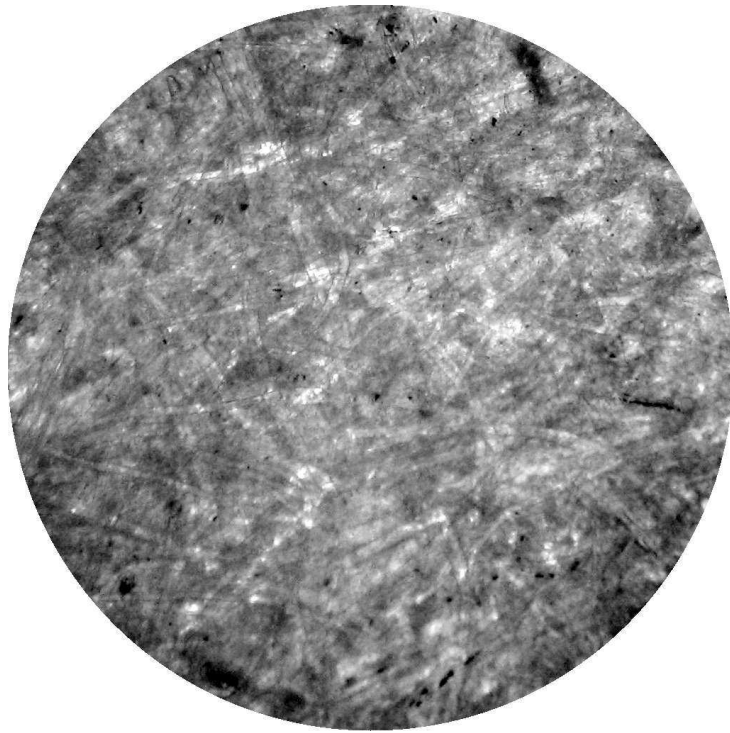


Figure 5: An optical transmission image of a piece of newsprint paper.

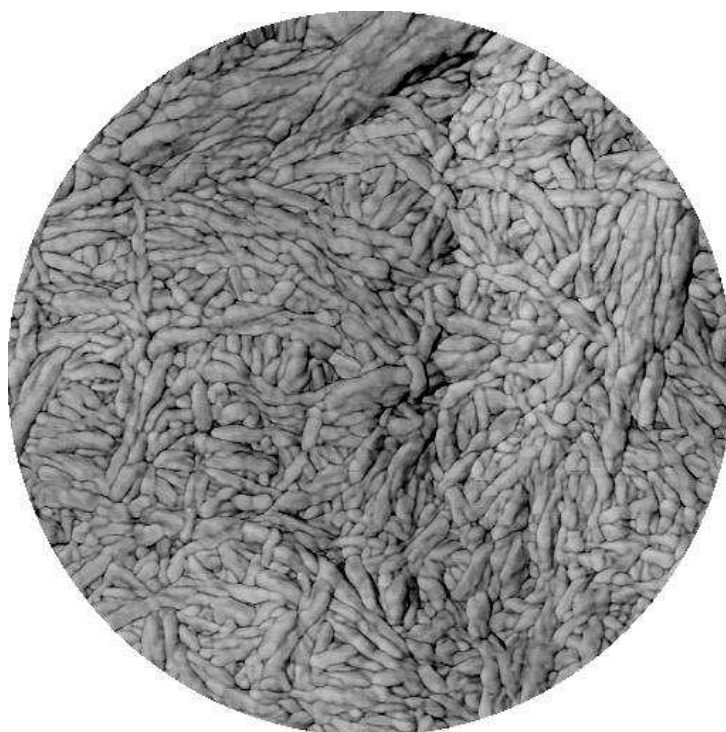


Figure 6: An atomic-force-microscopy (AFM) image of a thin film made of organic nanofibrils.

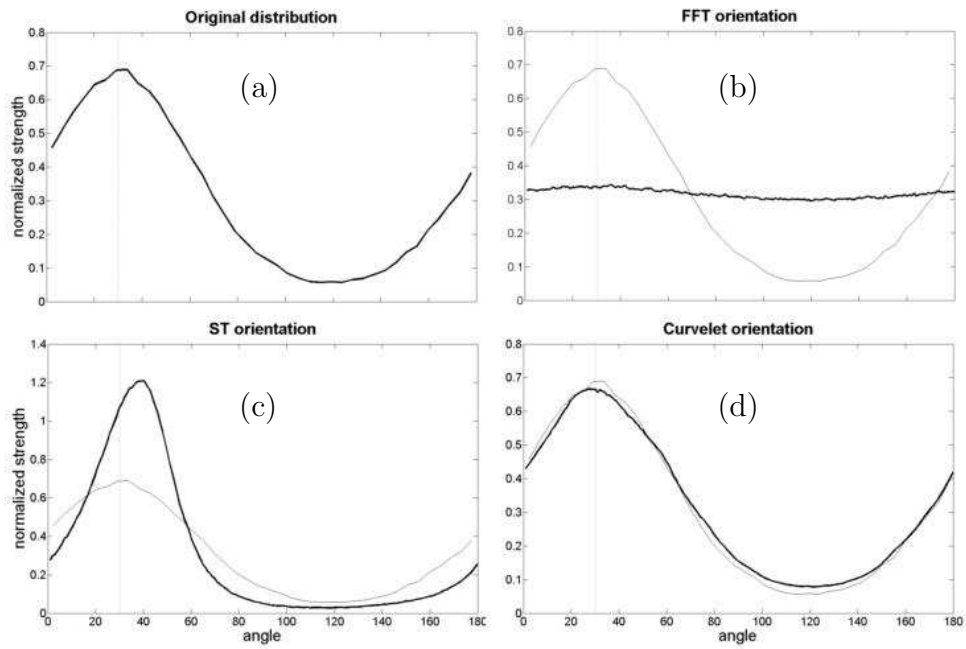


Figure 7: Distribution of fiber orientation in the image of a numerically generated network of fibers shown in (Fig. 4). (a) The known distribution in the generated network. (b) Orientation distribution as determined by the FFT method. (c) Orientation distribution as determined by the ST method. (d) Orientation distribution as determined by the curvelet method. The original distribution is plotted using gray line also in panels (b)-(d) for comparison.

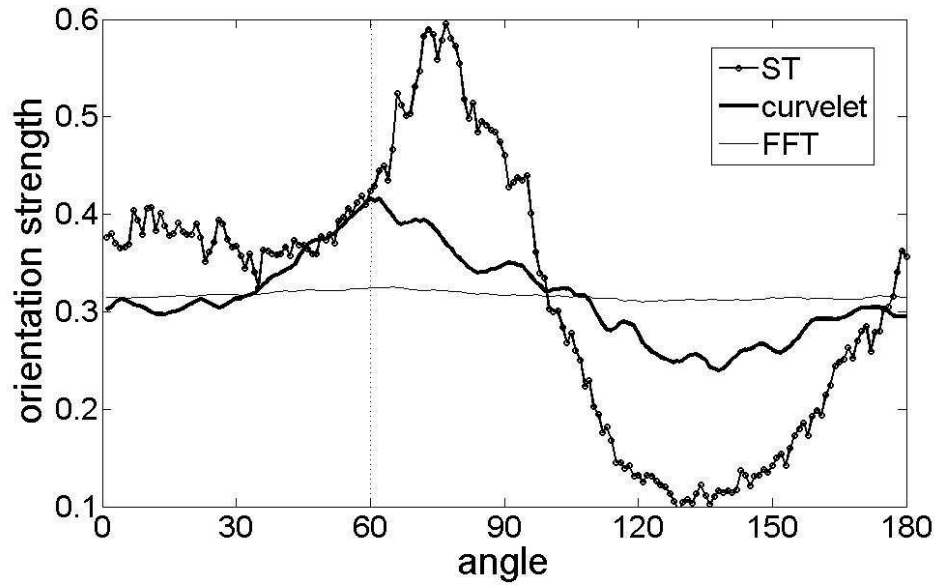


Figure 8: Three estimates for the fiber-orientation distribution from the optical-transmission image of newsprint shown in Fig. 5.

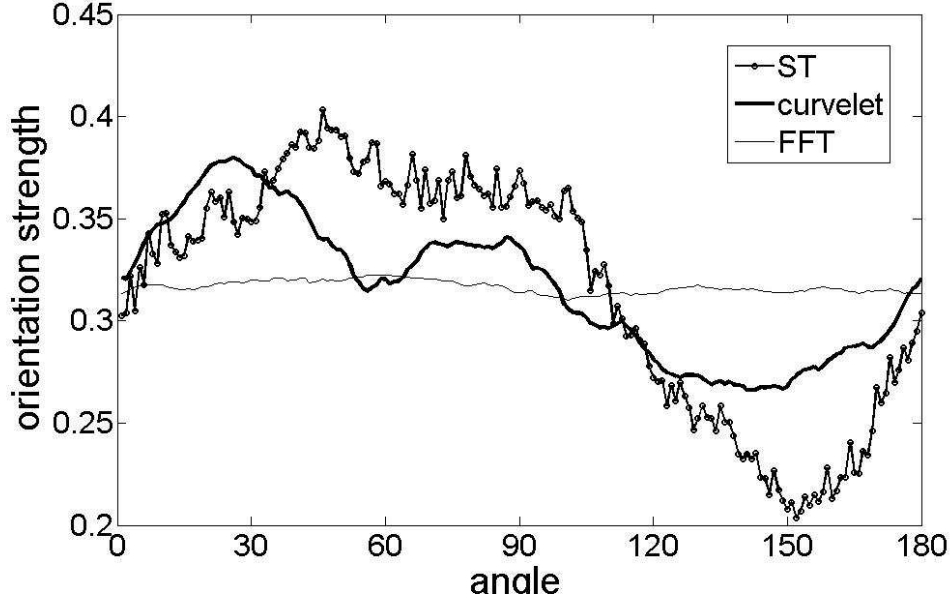


Figure 9: Three estimates for the fiber-orientation distribution in the AFM image of organic nanofibrils shown in Fig. 6.

#### 4.2. Discussion

Comparing the estimates for the distribution of fiber orientation as given by the three different methods considered with the actual distribution in the numerically generated network (an image in Fig. 7), it is evident that the curvelet-based method gives much better results than the ST and FFT methods. The main problem with the ST method is to find a good compromise between the overall distribution and the position of the maximum. With certain values of the most relevant parameters of the method, it is possible to get the position of the maximum almost right, but then the overall distribution would be much worse than one shown in Fig. 7. Notice that the ST method clearly overestimates the orientation strength. The main difficulty with the FFT method is exclusion of the base so as to get enough of variation between the maximum and minimum values of the distribution. In the present analyses, we did not do any subtraction of the base because there was no way to determine the exact baseline level. Also, there usually (when the base is subtracted) are noisy fluctuations in the FFT distribution curve, which, however, can be decreased by smoothing. In contrast with this, the

curvelet method seems to estimate the overall distribution quite well and to locate the maximum very accurately, even without any filtering of the image.

In Fig. 8 a similar comparison is made for an image of newsprint. When comparing the results of the curvelet and FFT methods, the former method seems to measure a much larger variation in the orientation strength. It is thus difficult to determine the exact angle of the orientation maximum by the FFT method without any prior information. The ST method seems to perform surprisingly badly on this image: locates, e.g., the maximum about twenty degrees away from its assumed value, and the orientation strength far too large for a newsprint. the reason for this is so far unclear. It might be that some features not related to orientation of fibers may influence the analysis of this sample. Notice that the ST method is somewhat blind to the scale of features in the image.

Comparison in Fig. 9 of the three orientation distribution estimates for the nanofibril image is more difficult to evaluate since there is no prior knowledge of the actual distribution. The appearance of two orientation maxima in the curvelet result, and less so clearly also in the ST result, is plausible by visual inspection of the image(Fig. 6). The orientation strength is largest in the ST result, and based on the results for the numerically generated network, it is expected that the ST result overestimates the strength. The FFT displays hardly any features as no baseline subtraction has been made. There is thus reason to expect that also in this case the curvelet estimate for the orientation distribution is the best one.

## 5. Conclusions

A new method was introduced here for estimating the orientation distribution in images of elongated features (particles). The estimate by this method for an image of known features was demonstrated to be very accurate, and to clearly outperform those by the FFT and ST methods used here to represent traditional orientation-analysis methods. There was also strong indication that the curvelet results for images of newsprint and organic nanofibrils were more reliable than the corresponding FFT and ST results.

The curvelet analysis of an image can be made very fast: we estimated and partly demonstrated (details not reported here) that such analysis can be implemented so that it only takes few milliseconds. This would allow on-line analysis with about 20 micrometer resolution in a paper machine with a web speed of 20 m/s. It is also evident based on the results reported above that

the curvelet method is robust and rather insensitive to noise in the image. this property strengthens its usability in practical applications.

### Appendix A. Proof of Theorem 3.3

It what follows a generic constant  $C$  is used, i.e., it can change from line to line. We also recall that  $\gamma$  and its derivatives have rapid decay and are  $C^\infty$  smooth.

Let us first concentrate on angles  $\hat{\theta} \geq Ca^{1/2}$ . If  $P$  is a polynomial function in the direction of  $S$ , then vanishing moments of  $\gamma$  imply that

$$\left| \int_{\mathbb{R}^2} f(x) \gamma_{ab\theta}(x) dx \right| = \left| \int_{\mathbb{R}^2} (f(x) - P(x)) \gamma_{ab\theta}(x) dx \right|.$$

Moreover, because the rapid decay of  $\gamma$ , for all  $N > 0$  there exists a constant  $C_N$  such that

$$\left| \int_{\mathbb{R}^2 \setminus B(b, r/2)} (f(x) - P(x)) \gamma_{ab\theta}(x) dx \right| \leq C_N a^N.$$

Therefore we have to find a bound only for the integral

$$\left| \int_{B(b, r/2)} (f(x) - P(x)) \gamma_{ab\theta}(x) dx \right|,$$

i.e., from now on we assume that  $x \in B(b, r/2)$ .

Let  $L_y$  be a line that is aligned with  $S$  and  $y$  be the intersection point of  $L_y$  and the major axis of  $\gamma_{ab\theta}$ . It is then possible to define a  $P(x)$  so that slice of  $P$  along  $L_y$  is always polynomial and there exists a constant  $C$  such that

$$|f(x) - P(x)| \leq C |x - y|^\beta$$

for all  $x \in L_y \cap B(b, r/2)$ . In particular, constant  $C$  is independent of  $y$ . This is a direct consequence from definition of Hölder regularity and the assumption that, in the direction of  $S$ , function  $f$  is  $C^\beta(B(b, r/2))$  smooth.

For simplicity, we first consider the integral over a small rectangle  $R$  (instead of  $B(b, r/2)$ ) centered in  $b$ , oriented like  $\gamma_{ab\theta}$  and having side lengths of  $a$  and  $a^{1/2}$ . First we notice that if  $x \in L_y \cap R$ , then

$$|x - y| \leq a / \sin \hat{\theta} \leq Ca / \hat{\theta}.$$

Therefore there exists a  $C < \infty$  such that

$$\begin{aligned}
& \left| \int_R (f(x) - P(x)) \gamma_{ab\theta}(x) dx \right| \\
& \leq \int_R |f(x) - P(x)| |\gamma_{ab\theta}(x)| dx \\
& \leq C a^{3/2} \left( a/\hat{\theta} \right)^\beta a^{-3/4} \\
& = C a^{3/4} \left( a/\hat{\theta} \right)^\beta.
\end{aligned}$$

Now we take a minimal collection of rectangles  $R_i$ , with similar size and orientation as  $R$ , but differently centered, such that  $R_i \cap R_j = \emptyset$  for  $i \neq j$  and  $B(b, r/2) \subset \cup_i R_i \subset B(b, r)$ . Similarly to the estimate above of the integral over  $R$ , using the decay Lemma 3.1, we find that

$$\left| \int_{R_i} (f(x) - P(x)) \gamma_{ab\theta}(x) dx \right| \leq C a^{3/2} \left( a/\hat{\theta} \right)^\beta \frac{a^{-3/4}}{1 + |D_{1/a} R_{-\theta}(c_i - b)|^{2N}},$$

where  $c_i \in \mathbb{R}^2$  is the center of  $R_i$ . Using this result we finally find that

$$\begin{aligned}
& \left| \int_{B(b, r/2)} (f(x) - P(x)) \gamma_{ab\theta}(x) dx \right| \\
& \leq C \sum_i a^{3/2} \left( a/\hat{\theta} \right)^\beta \frac{a^{-3/4}}{1 + |D_{1/a} R_{-\theta}(c_i - b)|^{2N}} \\
& \leq C a^{3/4} \left( a/\hat{\theta} \right)^\beta.
\end{aligned}$$

Now we can investigate what happens for angles  $\hat{\theta} \leq C a^{1/2}$ . Instead of considering slices in the direction of  $S$ , we consider slices in the direction perpendicular to the major orientation axis of  $\gamma_{ab\theta}$ , i.e., in the direction of vector  $R_\theta(1, 0)^\top$ . In this direction (like in any other direction)  $f$  is always  $C^\alpha$  and, if  $x \in L_y \cap R$ , then  $|x - y| \leq a$ . The rest of the calculations are exactly the same as in the case  $\hat{\theta} \geq C a^{1/2}$ .

## References

- [1] T. Enomae, Y.-H. Han, A. Isogai, Nondestructive determination of fiber orientation distribution of paper surface by image analysis, *Nordic Pulp and Paper Research Journal* 21 (2) (2006) 253–259.

- [2] T. Brox, R. van den Boomgaard, F. Lauze, J. van de Weijer, J. Weickert, P. Mrzek, P. Kornprobst, Adaptive structure tensors and their applications, in: J. Weickert, H. Hagen (Eds.), Visualization and Processing of Tensor Fields, Springer-Verlag, Berlin, pp. 17–47, 2006.
- [3] R. van den Boomgaard, J. van de Weijer, Robust estimation of orientation for texture analysis, The 2nd international workshop on texture analysis and synthesis, in conjunction with ECCV, Copenhagen, 2002.
- [4] S. K. Nath, K. Palaniappan, Adaptive robust structure tensors for orientation estimation and image segmentation, Lect. Notes Comput. Sci. 3804 (2005) 445–453.
- [5] M. Krause, J. M. Hausherr, B. Burgeth, C. Herrmann, W. Krenkel, Determination of the fibre orientation in composites using the structure tensor and local x-ray transform, J. Mater. Sci. (45) (2010) 888–896.
- [6] I. Daubechies, Ten lectures on wavelets, Society for Industrial and Applied Mathematics (SIAM), Philadelphia, PA, 1992.
- [7] E. J. Candès, D. L. Donoho, Recovering edges in ill-posed inverse problems: Optimality of curvelet frames, Ann. Stat. 30 (3) (2002) 784–842.
- [8] E. J. Candès, D. L. Donoho, New tight frames of curvelets and optimal representations of objects with piecewise  $C^2$  singularities, Commun. Pure Appl. Math. 57 (2) (2004) 219–266.
- [9] M. N. Do, M. Vetterli, The contourlet transform: An efficient directional multiresolution image representation, IEEE Trans. Image Process. 14 (12) (2005) 2091–2106.
- [10] K. Guo, D. Labate, Optimally sparse multidimensional representation using shearlets., SIAM J. Math. Anal. 39 (1) (2007) 298–318.
- [11] O. Wirjadi, K. Schladitz, A. Rack, T. Breuel, Applications of anisotropic image filters for computing 2D- and 3D-fiber orientations, in: V. Capasso, et al. (Eds.), Stereology and Image Analysis. Ecs10 - Proceedings of the 10th European Congress of ISS, The MIRIAM Project Series, volume 4, pp. 107–112, 2009

- [12] K. Niskanen, Paper Physics, Papermaking Science and Technology, Vol. 16, Fapet, Jyväskylä, 1998.
- [13] C. Antoine, P. Nygård, Ø. Weiby Gregersen, R. Holmstad, T. Weitkamp, C. Rau, 3D images of paper obtained by phase-contrast X-ray microtomography: image quality and binarisation, Nuclear Instruments and Methods in Physics Research Section A: Accelerators, Spectrometers, Detectors and Associated Equipment, Vol. 490, 1-2, 392–402, 2002.
- [14] E. J. Candès, D. L. Donoho, Continuous curvelet transform. I: Resolution of the wavefront set, Appl. Comput. Harmon. Anal. 19 (2) (2005) 162–197.
- [15] E. J. Candès, D. L. Donoho, Continuous curvelet transform. II: Discretization and frames, Appl. Comput. Harmon. Anal. 19 (2) (2005) 198–222.
- [16] J. Sampo, S. Sumetkijakan, Estimations of Hölder regularities and direction of singularity by hart smith and curvelet transforms, Journal of Fourier Analysis and Applications 15 (1) (2009) 58–79.
- [17] V. Brytik, M. V. de Hoop, M. Salo, Sensitivity analysis of wave-equation tomography: a multi-scale approach, Journal of Fourier Analysis and Applications 16 (4) (2010) 544–589.
- [18] J. Sampo, On convergence of transforms based on parabolic scaling, PhD. thesis, Lappeenranta University of Technology, <http://urn.fi/URN:ISBN:978-952-265-026-9>, 2010.
- [19] A. Ekman, A. Miettinen, T. Turpeinen, T. Timonen, The number of contacts in a random fiber networks, to be published, 2011.